Acta Oceanologica Sinica

Tracing the sources of nutrients through the Tsushima/Korea Strait

Jing Zhang, Xinyu Guo, Lei Zhu, Jianlong Feng, and Liang Zhao

View online: https://doi.org/10.1007/s13131-024-2372-1

Acta Oceanol. Sin., 2024, Vol. 43, No. 6, P. 142–152
https://doi.org/10.1007/s13131-024-2372-1
http://www.aosocean.com
E-mail: ocean2@hyxb.org.cn

Tracing the sources of nutrients through the Tsushima/Korea Strait

Jing Zhang[1, 2], Xinyu Guo[3], Lei Zhu[2], Jianlong Feng[1, 2], Liang Zhao[1, 2*]

[1] Key Laboratory of Marine Resource Chemistry and Food Technology, Ministry of Education, Tianjin 300457, China

[2] College of Marine and Environmental Science, Tianjin University of Science and Technology, Tianjin 300457, China

[3] Center for Marine Environmental Studies, Ehime University, Matsuyama 790-8577, Japan

Received 25 December 2023; accepted 7 May 2024

Abstract

The nutrients from the East China Sea (ECS) through the Tsushima/Korea Strait (TS) strongly impact the ecosystem of the Japan Sea (JS). The complex origins of the Tsushima Warm Current and the various nutrient sources in the ECS result in complex spatial-temporal variations in nutrients in the TS. Using a physical-biological model with a tracking technique, we studied the effects of nutrient sources from the ECS on the TS. Among all the nutrient sources, the Kuroshio has the highest nutrient concentrations in the TS. Its maximum concentration occurs at the bottom, while those of rivers and atmospheric deposition occur at the surface, and that of the Taiwan Strait occurs in the middle layer. The nutrient transport through the TS exhibits similar seasonal variations, as does the volume transport. The transport of nutrients from the Kuroshio accounts for more than 85% of the total. The transport of nutrients from the Taiwan Strait is greater during autumn and winter. The transport of dissolved inorganic nitrogen (DIN) from both rivers and atmospheric deposition through the TS peak in August. Nutrient transport cannot be equated with volume transport. The DIN in the less saline zone originates not only from rivers but also from atmospheric deposition and the Kuroshio. The transport of nutrients from the Taiwan Strait is not as significant as its volume transport in the TS.

Key words: dissolved inorganic nitrogen, dissolved inorganic phosphate, East China Sea, Japan Sea, nutrient transport

Citation: Zhang Jing, Guo Xinyu, Zhu Lei, Feng Jianlong, Zhao Liang. 2024. Tracing the sources of nutrients through the Tsushima/Korea Strait. Acta Oceanologica Sinica, 43(6): 142–152, doi: 10.1007/s13131-024-2372-1

1 Introduction

The Tsushima/Korea Strait (TS) is the connection between the East China Sea (ECS) and the Japan Sea (JS), two highly productive marginal seas in the western North Pacific Ocean (Kwak et al., 2014; Yamada et al., 2005; Lee et al., 2009). Tsushima Island divides the strait into eastern and western channels (ETS and WTS). Currents through the TS, mainly the Tsushima Warm Current (TWC), transport large amounts of water, heat, and materials from the ECS to the JS (Yanagi, 2002; Kodama et al., 2015). The nutrients supplied from the TS, especially, support 70%–80% of primary production in the coastal regions of the JS and have a great impact on the ecological environment in the JS (Onitsuka et al., 2007; Shibano et al., 2019).

The currents through the TS show strong spatial and temporal variations. The average volume transport is 2.64×10^6 m^3/s according to long-term ADCP measurements (Shin et al., 2022). The properties in the TS are influenced by many water masses upstream. Due to the connectivity among the straits over the western North Pacific Ocean, the Taiwan Warm Current and the Kuroshio are the main sources of the water flowing through the TS (Teague et al., 2003). Isobe (1999) suggested that the TWC originates from the Taiwan Strait, except in the fall when the Kuroshio branch southwest of Kyushu is strong and takes its place. By passive tracer experiments in a numerical model, Guo et al. (2006) found that in summer, the proportions of water from the Kuroshio and the Taiwan Strait in the TS are equal, but in winter, the ratio becomes 80% and 20%, respectively. Cho et al. (2009) also obtained similar ratios for the Kuroshio and the Taiwan Warm Current. Thus, the circulation patterns here are complex and characterized by the interaction between shelf water and the Kuroshio.

The TWC brings large amounts of nutrients from the ECS to the JS. Based on a box model, Zhang et al. (2007) estimated that the dissolved inorganic nitrogen (DIN) fluxes through the TS are 14.2 kmol/s and 18.1 kmol/s in summer and winter, respectively. The DIN fluxes transported through the ETS in summer-autumn are approximately 4.5–4.7 kmol/s, accounting for more than 60% of the total transport in a year (Morimoto et al., 2009). The transport of DIN through the western channel is comparable to that through the eastern channel, with an even greater flux density (Wang et al., 2019).

Complex water sources result in a wide variety of nutrient sources. In addition to the Kuroshio and Taiwan Strait, nutrients are also supplied from rivers and atmospheric deposition. Furthermore, several rivers from China and Korea's coasts enter the JS through the TS (Isobe et al., 2002). The main river is the Changjiang River, which contributes approximately 1% of the volume transport across the TS, with an annual mean discharge of 0.03×10^6 m^3/s. Approximately 68% of the Changjiang Diluted

Foundation item: The National Natural Science Foundation of China under contract Nos 42006018, 41876018 and 42176198; the Grants-in-Aid for Scientific Research [MEXT KAKENHI] under contract No. 22H05206; the Tianjin Municipal Education Commission Scientific Research Project under contract No. 2019KJ219.

*Corresponding author, E-mail: zhaoliang@tust.edu.cn

Water (CDW) extends to the TS during summer (Chang and Isobe, 2003). Because riverine nutrients usually exhibit high concentrations, the CDW is thought to be a significant nutrient source for nutrients in the middle and outer shelves of the ECS in summer (Kim et al., 2009; Bi et al., 2018). To what extent the riverine nutrients affect the TS and even the JS is unknown, atmospheric deposition is thought to be crucial to the health of ecosystems in the western North Pacific Ocean and has recently gained increasing attention (Kim et al., 2011). With a dramatically high N/P ratio, the excess DIN from atmospheric deposition in the ECS can be transported to the JS through the TS. While, Kim et al. (2013) thought the nutrients from Changjiang River contributed more than the atmospheric deposition.

Both complex hydrodynamics and various nutrient sources result in complex spatial-temporal variations in nutrients in the TS. It is also unknown which and to what extent the nutrient sources from the ECS affect the JS through the TS. In this study, we investigated the nutrient sources in the TS by a tracking technique with a physical-biological model. Section 2 provides a description of the method and model validation. Section 3 presents the distributions of the nutrient concentrations and fluxes at the TS and the seasonal variations in nutrient transport through the TS. Section 4 discusses the role of different nutrient sources in the TS and the JS. Section 5 presents a summary of this study.

2 Methods

2.1 *Physical-biological coupled model with a tracking technique*

The model domain spans the Bohai Sea, the Yellow Sea, and the ECS between 24°N and 41°N and between 117.5°E and 131.5°E (Fig. 1). The model is composed of a hydrodynamic module and a biological module. The hydrodynamic module is based on the Princeton Ocean Model, with a horizontal resolution of (1/18)° and a sigma level of 21. The low-trophic-level biological module was constructed for the ECS based on NORWECOM (Skogen et al., 1995; Skogen and Søiland, 1998). The configurations of the model in this study are generally the same as those of Zhao and Guo (2011) and Wang et al. (2019). The differences lie in the hydrological boundary conditions, which are changed to update the regional model results. The biological module takes into account three nutrients—DIN, dissolved inorganic phosphorus (DIP), and silicate; two phytoplankton species (CHL)—diatom (DIA) and flagellate (FLA); and two biogenic organic materials—dead organic matter (DET) and biogenic silica. Phytoplankton growth depends on nutrients, light and temperature. Detritus species include dead phytoplankton. The nutrients are restored via detritus remineralization and phytoplankton respiration. The dissolved organic phosphorus is not included in the biological model, which may affect the utilization of the phytoplankton (Jin et al., 2024).

The physical-biological coupled model is forced under climatological conditions. When the steady state of the model is reached, the tracking model is loaded. The tracking model was established based on Ménesguen et al. (2006) and has been applied to areas such as the ECS (Zhang et al., 2019, 2021; Große et al., 2020) and the JS (Onitsuka et al., 2007). The biological state variables share the same governing equations as the biological module but are calculated separately from different external sources. The state variables from each source are handled by a whole subset of equations (Eqs (1)–(4)). Since the physical pro-

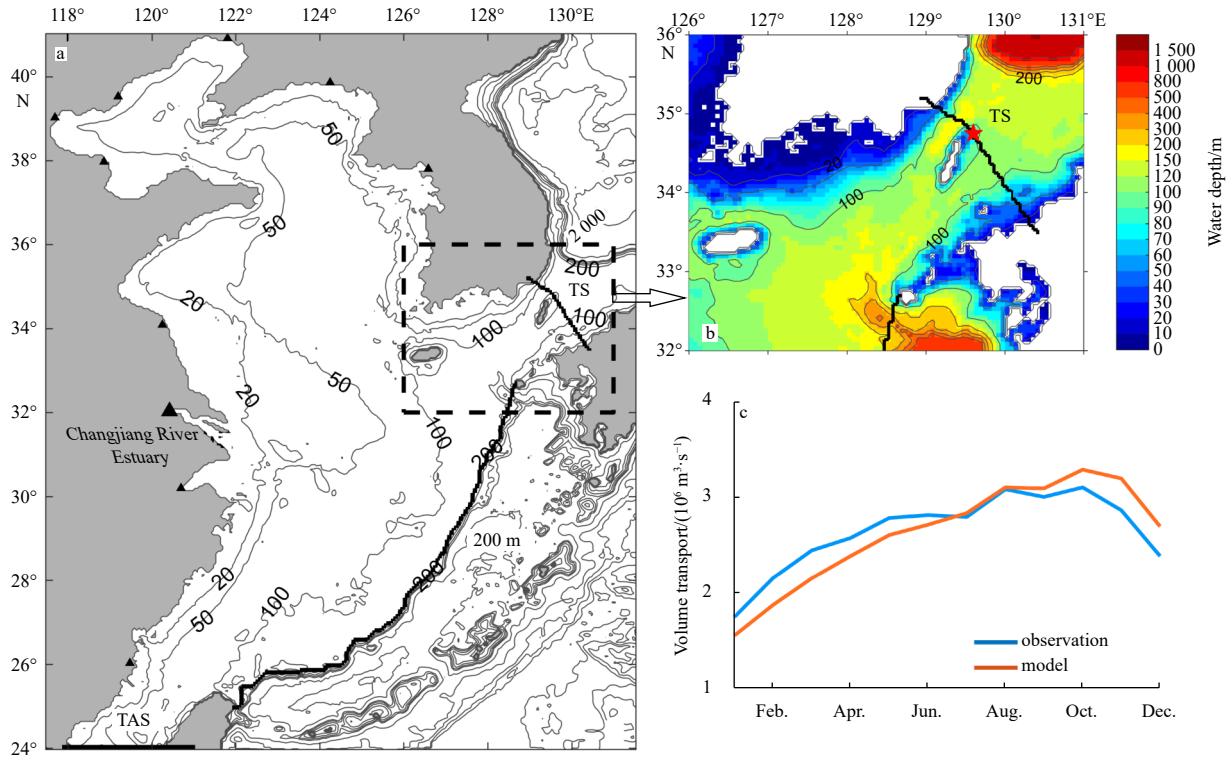

Fig. 1. Model bathymetry in the East China Sea and location of the Tsushima Strait section (TS), the Taiwan Strait section (TAS), and the 200-m isobath (200 m) (a). b. The dashed-line encircled area in Fig. 1a is displayed. The red pentagram marks the boundary between the eastern (ETS) and western (WTS) channels. The locations of the ETS and WTS are described previously by Takikawa et al. (2005). c. Monthly variations in volume transport through the TS. Red and blue represent the model and observation results, respectively.

cesses for the state variables are approximately linear, the advection and diffusion terms are separated for each source of variables. The biological processes were divided according to the proportion of the nutrient concentration of each source to the overall concentration.

The primary four external sources of DIN and DIP in the ECS are atmospheric deposition (A), the Taiwan Strait (T), the Kuroshio (K), and rivers (R). The two limiting nutrients in the ECS, DIN and DIP, are tracked in two cases. The nitrogen or phosphate cycle of each source is handled separately via separate equations. As an illustration, DIN_K represents the DIN concentration from the Kuroshio. By assimilating DIN_K, phytoplankton create CHL_K. CHL_K turns into DET_K after mortality. Further decomposition of DET_K results in the regeneration of DIN_K.

$$\frac{\partial \mathrm{DIN}_i}{\partial t} = \mathrm{diff}\left(\mathrm{DIN}_i\right) - \mathrm{adv}\left(\mathrm{DIN}_i\right) + \mathrm{resp}\left(\mathrm{FLA}\right) \times \frac{\mathrm{FLA}_i}{\mathrm{FLA}} + \mathrm{resp}\left(\mathrm{DIA}\right) \times \frac{\mathrm{DIA}_i}{\mathrm{DIA}} - \mathrm{pp}\left(\mathrm{FLA}+\mathrm{DIA}\right) \times \frac{\mathrm{DIN}_i}{\mathrm{DIN}} + \mathrm{remi}\left(\mathrm{DET}_i\right), \tag{1}$$

$$\frac{\partial \mathrm{DIA}_i}{\partial t} = \mathrm{diff}\left(\mathrm{DIA}_i\right) - \mathrm{adv}\left(\mathrm{DIA}_i\right) + \mathrm{pp}\left(\mathrm{DIA}\right) \times \frac{\mathrm{DIN}_i}{\mathrm{DIN}} - \mathrm{resp}\left(\mathrm{DIA}\right) \times \frac{\mathrm{DIA}_i}{\mathrm{DIA}} - \mathrm{mort}\left(\mathrm{DIA}_i\right), \tag{2}$$

$$\frac{\partial \mathrm{FLA}_i}{\partial t} = \mathrm{diff}\left(\mathrm{FLA}_i\right) - \mathrm{adv}\left(\mathrm{FLA}_i\right) + \mathrm{pp}\left(\mathrm{FLA}\right) \times \frac{\mathrm{DIN}_i}{\mathrm{DIN}} - \mathrm{resp}\left(\mathrm{FLA}\right) \times \frac{\mathrm{FLA}_i}{\mathrm{FLA}} - \mathrm{mort}\left(\mathrm{FLA}_i\right), \tag{3}$$

$$\frac{\partial \mathrm{DET}_i}{\partial t} = \mathrm{diff}\left(\mathrm{DET}_i\right) - \mathrm{adv}\left(\mathrm{DET}_i\right) + \mathrm{mort}(\mathrm{FLA}_i) + \mathrm{mort}(\mathrm{DIA}_i) - \mathrm{remi}\left(\mathrm{DET}_i\right), \tag{4}$$

where the subscript *i* represents the DIN from the *i*th source. The adv and diff represent the physical terms advection and diffusion. The resp, pp, remi, and mort indicate the biological terms respiration, primary production, remineralization, and mortality. The advection and diffusion terms are separated for each source of variables. The terms for biological processes are separated following the ratio of each source of DIN concentration to the total DIN concentration.

The lateral boundary conditions for nutrients from the Taiwan Strait were provided by Prof. Chen-Tung Arthur Chen (personal communication), and those for the Kuroshio east of Taiwan Island were obtained from the Japan Meteorological Agency observation data. The nutrient concentrations for ten rivers were obtained from observations at 1980s (Zhang, 1996; Liu et al., 2009). The nitrogen concentration of wet atmospheric deposition and dry atmospheric deposition flux were from observations around 2000s (Zhang et al., 2011), and for phosphate were averaged from limited observed data in the 1960s–2000s (Zhang and Liu, 1994; Chung et al., 1998; Liu et al., 2000; Zhang et al., 2004). The model area is divided into three regions: the Bohai Sea, Yellow Sea and ECS, and a single value for phosphorus atmospheric deposition without temporal and spatial variations is given for each region. So, the simulation presents a climatological state of the ecosystem in the ECS before the 2000s. At the start of the tracking model run, the DIN or DIP concentration, phytoplankton concentration, and detrital concentration of the four external sources are all set to zero. Until the tracking state variables reached a stable state, the tracking module was run for more than 5 years. The results from the last year are examined in this study.

2.2 *Validation of the model results in the TS*

The ability of the physical-biological coupled model to reproduce the seasonal variations in physical and biological variables across the ECS has been fully confirmed by Zhao and Guo (2011), Wang et al. (2019), and Shen et al. (2021). Wang et al. (2019) reported good agreement between the modeled and measured vertical distributions of DIN and CHL concentrations across the ETS (Morimoto et al., 2009). The concentrations of DIN and CHL in a section in the northern ECS (i.e., the section upstream of the TS) from the model results shown by Zhang et al. (2019) were similar to previous observations (Umezawa et al., 2014). The tracking model has also been used to evaluate the roles of nutrients from different sources in ecosystems of the ECS (Zhang et al., 2019, 2021).

The section of the TS (Fig. 1b) is designed to be the same as the observation line in Takikawa et al. (2005). The red pentagram separates the eastern and western channels. Here, we mainly focus on the validation of the model results in section TS. A comparison of the volume transport through section TS from the model results and observations (Shin et al., 2022) is shown in Fig. 1c. Both of them are highest in October and lowest in January, suggesting similar seasonal variations. The annual means of the volume transport from the model results and observations are 2.62×10^6 m^3/s and 2.64×10^6 m^3/s, respectively, whose differences are less than 1%.

Then, we compare the vertical distributions of the velocity that is normal to the section, as well as the temperature, salinity, DIN concentration, DIP concentration, and CHL concentration in the TS section from the model results (Fig. 2) with the observations in the ETS in August and October from Morimoto et al. (2009). The velocities from both the model and observation results in August are the greatest (more than 20 cm/s) where the water depth is the greatest in the ETS (Fig. 2a). On the western side of this current core, a countercurrent appears with similar strength. The pattern of currents in October is comparable to that in August but with a weaker countercurrent (Fig. 2b). The core regions of both the WTS and ETS have two northeastward current maximums, with the maximum velocity of the WTS being greater than that of the ETS. The temperature in August is stratified according to either the observations or the model results (Fig. 2c). The surface temperature is higher than 24℃, and the bottom temperature is less than 12℃. In October (Fig. 2d), the stratification in the upper 40-m layer of the ETS decays, and the bottom temperature increases compared to that in August. In August, the salinity is relatively low in the surface layer on the western side of the TS, with observations and model results of approximately 31 (Fig. 2e). The highest salinity is greater than 34.2. The low-salinity zone narrows in October and is confined only to the upper WTS (Fig. 2f). The discharge of freshwater from the Changjiang River in the ECS is the most likely cause of the low salinity in the WTS from August to October (Chen et al., 1994; Takikawa et al., 2005). The vertical variations in salinity in the ETS are small and are also relatively consistent with the observations.

The chlorophyll concentration in August clearly reaches a maximum in the subsurface layer according to both the observation and model results, with concentrations greater than 1 mg/m^3 (Fig. 2g). However, in October, the chlorophyll concentrations above a depth of 50 m are relatively high according to both the

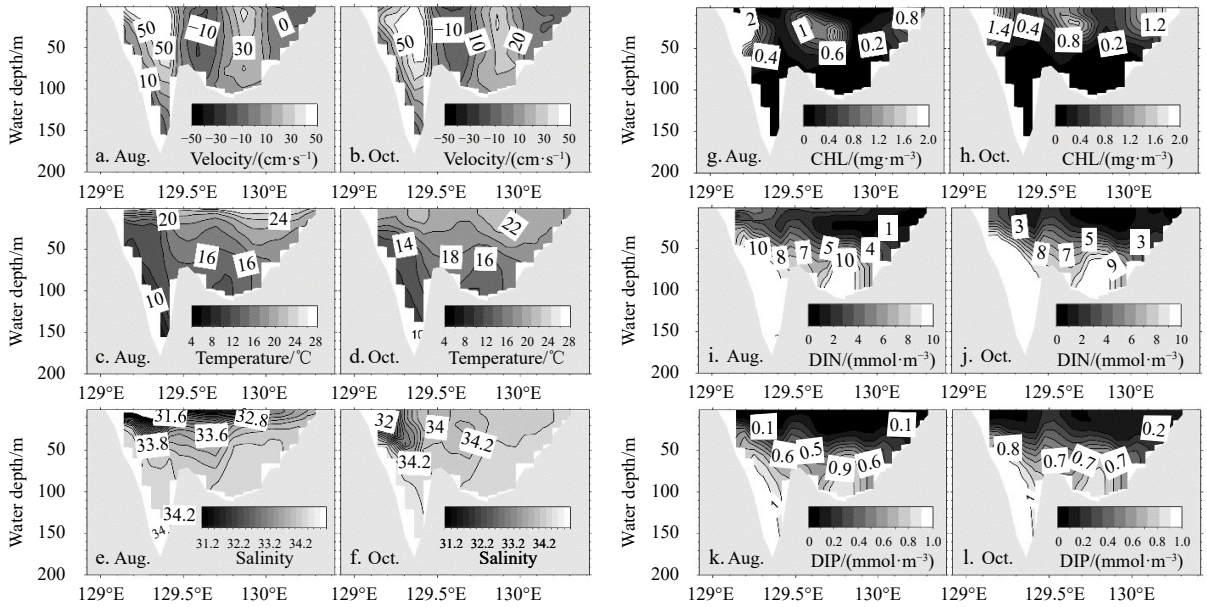

Fig. 2. Vertical distributions of the velocity normal to the section (cm/s) (a, b), the temperature (℃) (c, d), the salinity (e, f), the CHL concentration (mg/m³) (g, h), the DIN concentration (mmol/m³) (i, j) and the DIP concentration (mmol/m³) (k, l) in the TS section in August and October from the model results. A positive velocity indicates transport in the direction from the ECS to the JS.

observation and model results, with a maximum in the ETS coastal zone (Fig. 2h). The minimum DIN concentration in August is less than 1 mmol/m³, and the maximum DIN concentration is greater than 10 mmol/m³. Both the variation and the vertical structure are consistent with the observations (Fig. 2i). The range of change in the DIN concentration in October is comparable to that in August, except that the gradient is less pronounced in the vertical direction; in particular, there is little variation in the low-concentration zone in the upper 40 m layer (Fig. 2j). The distributions of DIP in the TS are generally comparable to those of DIN. The minimum DIP concentration is lower than 0.1 mmol/m³, and the maximum DIP concentration is higher than 0.8 mmol/m³ (Figs 2k and l).

3 Results

3.1 *Vertical distributions of DIN and DIP concentrations in the TS section*

Figure 3 displays the vertical distribution of DIN from each source. The four columns, which correspond to the four seasons, are February, May, August, and November. One DIN source appears in each row, and the total DIN (DIN_W) appears in the final row.

The DIN_R appears in the first row. From winter to spring, the concentration is quite low across the whole section. The highest DIN_R concentration (up to 2 mmol/m³) is found in the upper 50-m layer of the WTS in summer, mainly resulting from the strong northeastward CDW. The DIN_R concentration in the surface layer of the middle ETS is also greater than 0.50 mmol/m³. In autumn, the DIN_R high-concentration zone is located in the coastal WTS, and its concentration decreases compared to that in summer with the retreating CDW.

The concentration of the DIN_A is slightly greater than that of the DIN_R. In winter, the high-value region is concentrated in the lower layer of the WTS. These DIN_A are not newly supplied from the sea surface but instead are locally regenerated or/and remotely conveyed. In spring, the DIN_A has an unapparent three-layer structure in both the WTS and ETS, with a greater concentration in the top 10 m layer and around the bottom layer. In summer, there is a noticeable increase in the DIN_A concentration in the upper layer of the entire TS section due to the strong atmospheric deposition input. The patterns of the DIN_A throughout the fall are identical to those of the DIN_R.

The DIN_K concentration was the highest of the four DINs. Its content in winter is an order of magnitude greater than that of the other DINs, ranging from 3 mmol/m³ to 6 mmol/m³. The DIN_K is vertically uniform throughout the whole section due to strong vertical mixing. In the spring, the concentration disparity between the top and bottom layers increases in both channels, especially in the ETS. The maximum concentration of DIN_K (at least 8 mmol/m³) in spring occurs in the bottom layer of the ETS. In summer, the bottom of both channels exhibits a high concentration of DIN_K. In autumn, the DIN_K again mixes well within the upper 50-m layer in the vertical direction. The DIN_K in the lower layer is always greater than that in the upper layer, in contrast to the DIN_R, DIN_A, and DIN_T. However, the nutrients at the Kuroshio main axis show the similar patterns (Guo et al., 2012). The Kuroshio intrusion through the TS section is also stronger at the bottom (Guo et al., 2006).

The DIN_T has little seasonal or vertical fluctuation and is on the same level as the DIN_R and DIN_T. Its concentration and distribution pattern during the winter and spring are comparable to those of DIN_A. The main difference between them is that they lack a high value in the surface layer in spring. During the summer, the DIN_T concentration does not substantially differ across the entire section. In the WTS, a weak, highly concentrated core can be observed at a depth of approximately 50 m rather than at the surface layer, as in the DIN_R and DIN_A, or at the bottom layer, as in the DIN_K. In the autumn, the content of the DIN_T summer core increases to more than 0.9 mmol/m³. In contrast, the DIN_T is typically vertically homogenous in the ETS. The DIN_T concentration reaches its peak in autumn, whereas DIN_T transport through the Taiwan Strait is the greatest in summer following volume transport.

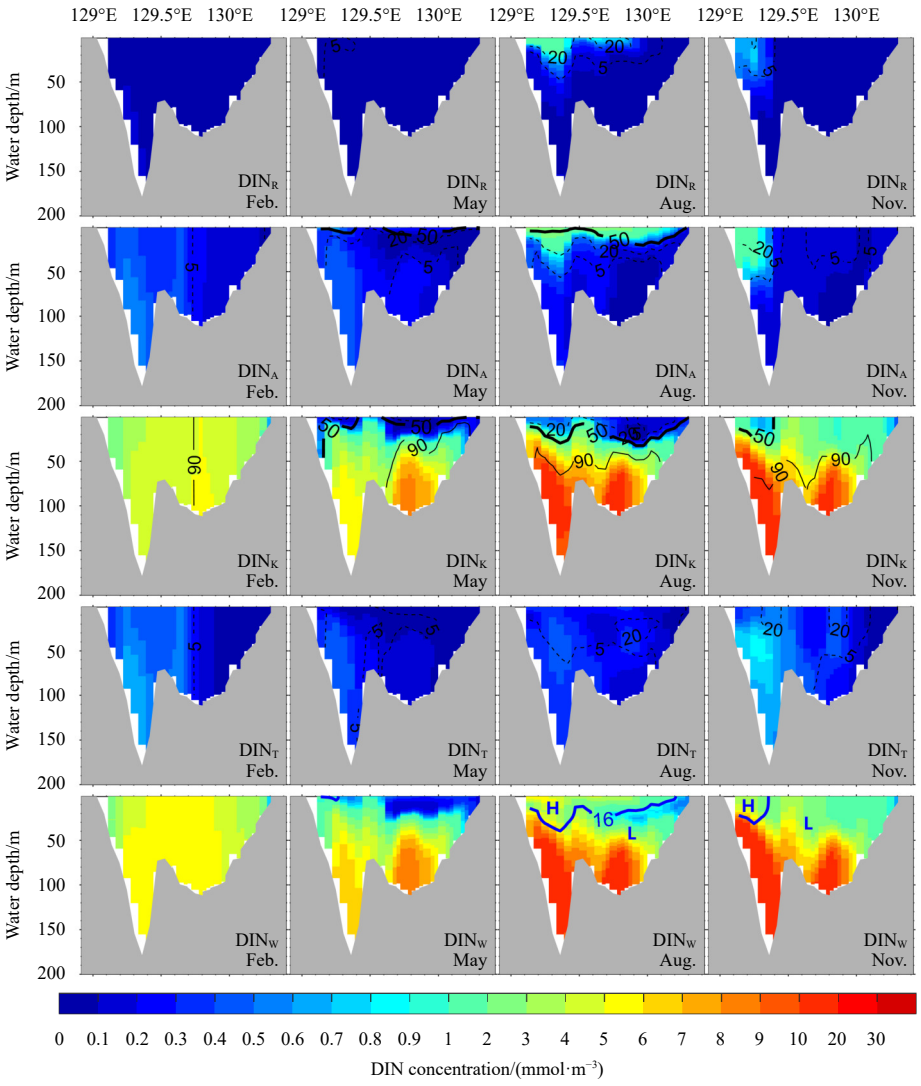

Fig. 3. Vertical distributions of DIN (mmol/m^3) in the TS from rivers (DIN$_R$), the atmosphere (DIN$_A$), the Kuroshio (DIN$_K$), the Taiwan Strait (DIN$_T$), and the sum of the four sources (DIN$_W$) in four seasons. The proportion of DIN from a single source to DIN$_W$ is shown by the black contour lines in the first four rows. The black dash lines indicate 5% and 20%. The thin black line represents 90%. The thick black line represents 50%, which suggests the dominant role of the DIN source. The blue contours in the last row denote an N/P ratio of 16. The letters "H" and "L" represent N/P ratios higher than 16 and lower than 16, respectively.

The proportion of DIN from a single source to DIN$_W$ is shown by the black contour lines in the first four rows. The DIN$_R$ reaches more than 20% in only limited areas of the upper 20-m layer in summer. Otherwise, its proportion is low, especially during the winter, when it decreases to less than 5%. Although DIN$_A$ is low in winter as well, it makes up more than half of the DIN$_W$ in the upper 10-m layer in spring and the upper 20-m layer in summer. The percentage of DIN$_A$ drops as the water depth increases.

Almost the entire section is under DIN$_K$ dominance during the winter. This dominance is also present in the spring at a layer deeper than 20 m in the ETS and in the summer and fall at the bottom 50 m layer. As the water depth increases, the proportion of DIN$_K$ also increases. The percentage of DIN$_T$ is only approximately 5% in winter and spring and is as low as that of DIN$_R$. In the middle layer of the ETS during summer and in the middle layers of the WTS and ETS during fall, there is a tiny cluster of DIN$_T$ with more than 20% occupancy. However, temporally and spatially, it makes minimal contributions to the DIN$_W$ during the rest of the period.

The DIN$_W$ concentration exhibits nearly identical seasonal variations to those of DIN$_K$, which is the predominant concentration. The DIN$_W$ mixes well in the top 50-m layer throughout the winter. As a result of the vigorous primary production in spring, the DIN$_W$ concentration in the upper 30-m layer decreases. The DIN$_W$ concentration increases in the bottom layer and peaks in summer. The DIN$_W$ develops a core with a greater concentration in the upper 10-m layer due to the combined impact of the DIN$_R$ and DIN$_A$ near the surface of the WTS in summer. In autumn, the DIN$_W$ in the upper layer barely changes in the vertical direction. The DIN$_W$ concentration in the western channel is greater than that in the eastern channel due to the greater water depth and the intrusion of a water mass with high DIN concentrations from the JS (Shibano et al., 2019).

An N/P ratio of 16 is indicated by the blue contours in the final row for reference. The letters "H" and "L" represent N/P ratios higher than 16 and lower than 16, which correspond to the limiting nutrients, phosphate and nitrogen, respectively. In winter and spring, the N/P ratios in the whole section range from

2 to 12, indicating a nitrogen limitation. However, in the upper 20~30 m layer in summer and the upper 20 m layer of the WTS in autumn, the N/P ratio is greater than 16. Overall, nitrogen is the potential limiting factor for primary production in section TS.

The DIP concentrations of the different sources in section TS are shown in Fig. 4. Both the DIP_R and DIP_A concentrations in section TS are very low, with values less than 0.005 mmol/m^3 due to the high N/P ratios of both atmospheric deposition and riverine sources (Zhang et al., 2007).

However, DIP_K is the complete opposite of DIP_R and DIP_A; hence, DIP_K occupancy is substantially greater than DIN_K occupancy. DIP_K is still vertically homogenous in winter and accounts for approximately 90% of the total occupancy. In comparison to DIN_K in spring, the low-concentration zone of DIN_K found in the surface layer does not develop for DIP_K. The surface layer is a nitrogen-limited area, and phosphorus is not used efficiently. The DIP_K in the ETS also had a concentration of more than 90% DIP_W. In summer, the concentration of DIP_K is less than half of the DIP_W in the upper 10 m at the WTS and upper 30 m at the ETS. DIP_K still comprises more than 90% of the total at depth below approximately 50 m in both channels. By autumn, the DIP_K concentration barely changes in the lower layer, while the DIP_K concentration in the upper layer rises and returns to springtime levels.

In winter, spring, and fall, the DIP_T concentration in the WTS is greater than that in the ETS. The maximum value is observed at the same location as that of DIN_T, which is at a depth of approximately 50 m in the coastal zone adjacent to the WTS, and the DIP_T accounts for more than 20% of the DIP_W in this area. However, in summer, the DIP_T concentration is greater in the ETS than in the WTS. It dominates the upper 40 m layer of the ETS with more than 50% occupancy, which is very different from the weak state of DIN_T.

While DIP_W and DIN_W exhibit different patterns, they are both characterized by vertical homogeneity in the winter and increasing concentrations with depth in the spring, summer, and fall. Differences between DIP_W and DIN_W are found in the various phosphorus and nitrogen limitation zones. The DIP_W concentra-

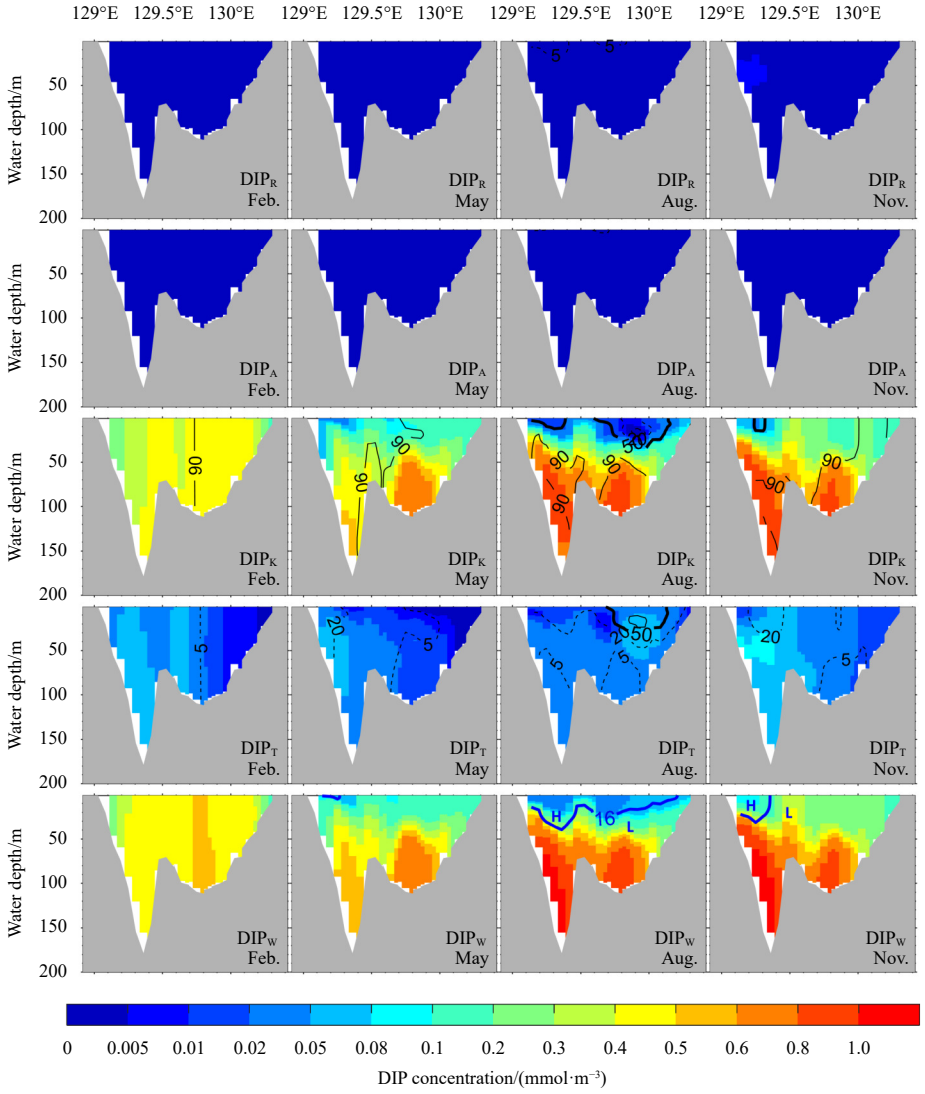

Fig. 4. Vertical distributions of DIP (mmol/m^3) in the TS from rivers (DIP_R), the atmosphere (DIP_A), the Kuroshio (DIP_K), the Taiwan Strait (DIP_T), and the sum of the four sources (DIP_W) in four seasons. The proportion of DIP from a single source to DIP_W is shown by the black contour lines in the first four rows. The black dash lines with 5 and 20 indicate 5% and 20%. The thin black line with 90 represents 90%. The thick black line with 50 represents 50%, which suggests the dominant role of the DIP source. The blue contours in the last row denote an N/P ratio of 16. The letters "H" and "L" represent N/P ratios higher than 16 and lower than 16, respectively.

tion does not significantly differ between the upper layer and the lower layer in spring when the entire section is nitrogen limited. At the same time, the DIN_W concentration decreases substantially in the euphotic layer due to primary production. Similarly, the DIP_W concentration greatly decreases throughout the summer in the phosphorus-limited area in the upper layer, where the DIN_W is in excess.

3.2 *Vertical distributions of DIN and DIP fluxes in the TS section*

To evaluate the effects of different nutrient sources on the ecosystem of the JS, the nutrient concentration in section TS alone is not sufficient. Hence, we present the vertical distributions of the DIN and DIP downstream fluxes in Figs 5 and 6. The nutrient flux is calculated as the product of the nutrient concentration and the velocity component normal to the section, demonstrating the vertical patterns of nutrient transport. A positive value indicates a northeastward nutrient flux entering the JS. The current structures in section TS exhibit weak seasonal variation. In the middle of the eastern and western channels, there are two maximums of the northeastward current (Figs 2e and f). The maximum velocity is greater in the WTS than in the ETS. Between the WTS and ETS, a southwestward countercurrent is present, which is associated with two cyclonic and anticyclonic eddies (Takikawa et al., 2005). Additionally, there are weak countercurrents at the bottom of the WTS in summer and autumn and in the eastern ETS.

The DIN flux is primarily in the JS direction since its positive area is wider and has greater flux values than does its negative area (Fig. 5). The DIN_R and DIN_A fluxes share similar vertical distributions. Their maximums (>0.5 mmol/(m²·s)) appear in summer at the surface of the WTS, where both the velocity and concentration are high.

During the winter, the DIN_K flux remains largely uniform in the vertical direction, with greater values in the center of the two channels. The DIN_K flux increases below a depth of 50 m after winter. The surface has a higher velocity, while the bottom has a higher DIN_K concentration. Hence, the core DIN_K flux lies between 50 m and 100 m deep, with the maximum occurring at a depth of 80 m in the WTS in autumn. The flux of DIN_T is at the same level as that of DIN_R and DIN_A. A weak core of the DIN_T flux appears at the 40-m depth of the WTS in autumn, which corresponds to the largest DIN_T concentration. The distribution of DIN_W is mostly similar to that of DIN_K, except for the upper layer in summer, which is superimposed on DIN_R and DIN_A and hence

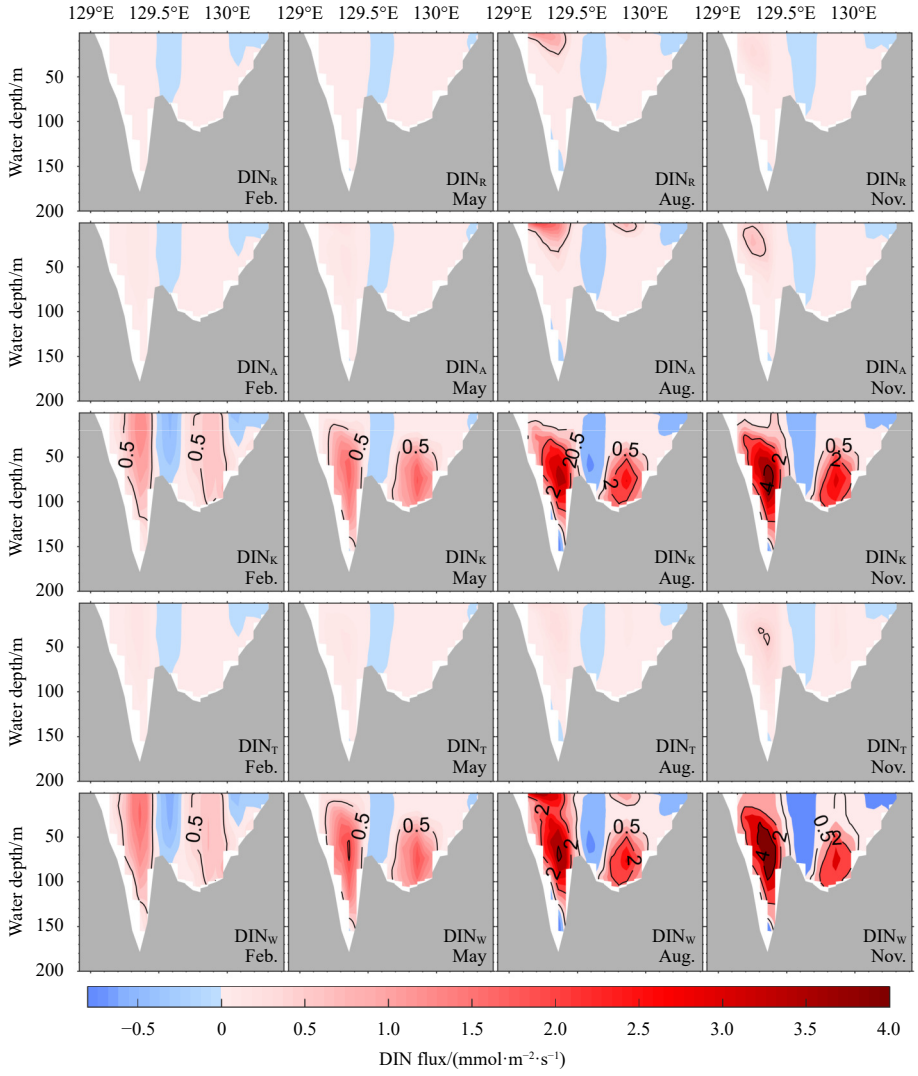

Fig. 5. Vertical distributions of DIN fluxes (mmol/(m²·s)) at the TS from rivers (DIN_R), the atmosphere (DIN_A), the Kuroshio (DIN_K), the Taiwan Strait (DIN_T) and the sum of the four sources (DIN_W) in four seasons.

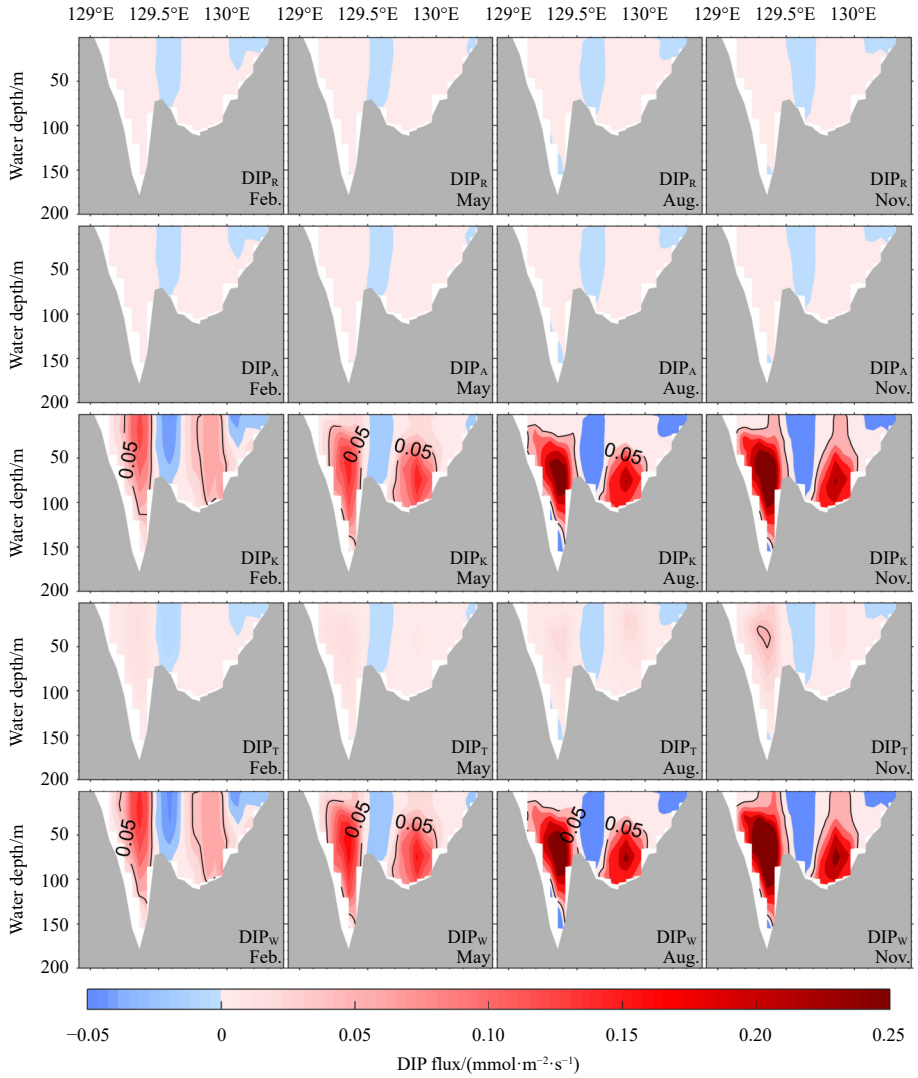

Fig. 6. Vertical distributions of DIP fluxes [mmol/(m²·s)] at the TS from rivers (DIP_R), the atmosphere (DIP_A), the Kuroshio (DIP_K), the Taiwan Strait (DIP_T) and the sum of the four sources (DIN_W) in four seasons.

has larger values. The positive DIN_W flux is the strongest in autumn, and the negative value between the two channels is also the largest due to the eddy effect.

The vertical distributions of DIP fluxes from different sources are shown in Fig. 6. Because of the low concentrations of DIP_R and DIP_A, their fluxes are similarly quite small. The patterns of the DIP_K flux are comparable to those of DIN_K. Although there is not much difference in DIP_K concentrations between the WTS and ETS, the WTS has a stronger flux because of the higher velocity. The DIP_T flux is slightly greater than that of DIN_R and DIN_A and peaks at the 50-m layer of the WTS in autumn as DIN_T. With the relatively minor effects of the other three DIP sources, the pattern of DIP_W fluxes is more consistent with that of DIP_K.

3.3 *DIN and DIP transports across the TS section*

The transport across the TS section is obtained by integrating the entire flux, as illustrated in Figs 5 and 6, which indicate the combined effect of volume transport and nutrient concentrations (Fig. 7). Figure 1c shows the seasonal fluctuations in volume transport, with a minimum in January and a maximum in October.

As shown in Fig. 7a, the transports of DIN_R, DIN_T, and DIN_A are at the same level. The mean values of these parameters, which correlate to the axis on the left, are 0.33 kmol/s, 0.87 kmol/s, and 0.97 kmol/s. In the winter and spring, the DIN_R transport is quite low. It starts to rise after May and reaches its peak in August. Freshwater transport through the TS increases noticeably in the summer and fall, two or three months after river discharge (Isobe et al., 2002). The seasonal trend of DIN_A transport is fairly similar to that of DIN_R, although the DIN_A values are almost three times greater. The DIN_T transport remains at a low level in spring and rapidly increases from June to a maximum in December. While volume transport from the Taiwan Strait is highest in summer, DIN_T transport peaks later.

The annual mean transport of DIN_K is 11.86 kmol/s, which is an order of magnitude greater than those of the other three sources and accounts for 85% of the total transport. Its seasonal oscillation is consistent with that of the volume transport, which is greatest in October and smallest in January. The DIN_W transport is 14.03 kmol/s, which is comparable to the estimated value of 16.20 kmol/s (Zhang et al., 2007). In winter and spring, almost all of the DIN_W transport comes from the Kuroshio, and in summer and fall, it is supplemented partly by atmospheric deposition, rivers, and the Taiwan Strait.

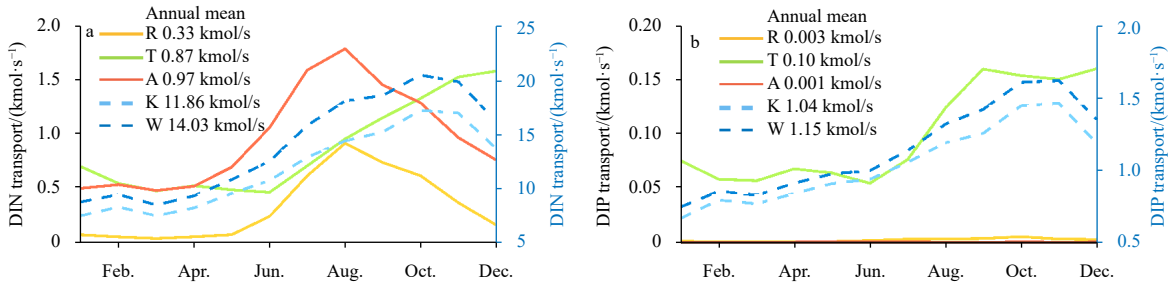

Fig. 7. DIN (a) and DIP (b) transport across the TS. R, A, T, K, and W represent nutrients from the river, atmospheric deposition, the Taiwan Strait, the Kuroshio, and total nutrients, respectively. The annual mean of each transport is shown behind these letters in the legend. The transports of nutrients from the Kuroshio and the total are indicated by the dashed line and correspond to the right *y*-axis.

The DIP_W transport has an annual mean of 1.15 kmol/s, which is similar to the value of 0.96 kmol/s from Zhang et al. (2007). The seasonal fluctuation in DIP_W is fairly similar to that in DIN_W, except that there is no slight peak in summer due to the small contributions from the atmosphere and rivers. The transports of DIP_A and DIP_R make up less than 0.50% of the total. With an annual mean of 1.04 kmol/s, the proportion of DIP_K transport reaches 90%. Its seasonal variations are similar to those of DIN_K. Similar to the DIN_T flux, DIP_T transport also begins to increase after June, and maintains high levels from September through December.

4 Discussions

4.1 *DIN nutrient sources in the less saline zone*

The less saline zone is found in the upper layer in summer and autumn (Figs 2e and f) and is considered to be associated with the CDW (Chang and Isobe, 2003). The CDW flows into the JS under the southeast monsoon in summer (Lie and Cho, 2016). The less saline zone corresponds to the zone with a high N/P ratio, where primary production is limited by DIP. The excess DIN in the TWC is thought to be affected by rivers in East Asia (Kodama et al., 2015, 2017).

According to our model results (Fig. 3), the DIN in the less saline zone originates not only from rivers (~20%) but also from atmospheric deposition (~50%) and the Kuroshio (~20%). The DIN_R does not have as much of an impact as the DIN_A does. The total input of DIN_R is 1.20 kmol/s, and the DIN_R transport through the TS is 0.33 kmol/s, accounting for only 28% of the input. Approximately 68% of the Changjiang River discharge is transported through the TS according to tracer experiments (Chang and Isobe, 2003). These two distinct ratios show that nutrient transport and freshwater transport cannot be equated.

While in this study, the nutrient input fluxes from the rivers remain consistent with our previous study (Zhang et al., 2019). The nutrient levels from the Changjiang River are observed value in the 1980s (Zhang, 1996), which is less than the values in recent years reported by Wu et al. (2023). A sensitivity experiment was designed specifically that changing the DIN concentration in Changjiang River from 110.20 mmol/m^3 to 33.50 mmol/m^3 (Zhang et al., 2021). With the increasing loading of Changjiang River DIN from the 1980s to the 2010s, the produced PON does not increase proportionally due to limited primary production. Consequently, residual DIN_R from the Changjiang River is transported further from the ECS to the JS, thereby increasing the environmental stress in the adjacent areas. The contribution of the DIN_R may be underestimated due to the low level of the input nutrient concentrations in the 1980s.

4.2 *Effects of the Kuroshio and the Taiwan Strait on nutrients in the TS*

The Taiwan Strait and the Kuroshio have a competing relationship when they act as the source waters of the Tsushima Warm Current. The Kuroshio branch southwest of Kyushu is the main source of the TWC in winter, while the Taiwan Warm Current also contributes to the TWC in summer (Ichikawa and Beardsley, 2002). According to a tracer experiment conducted by Guo et al. (2006), the Taiwan Strait contributes almost half of the tracer entering the Tsushima Strait during the summer, with the Kuroshio contributing the other half. The contribution from the Taiwan Strait decreases to 20%, and that from the Kuroshio increases to 80% from summer to winter. Although the volume transport in the Taiwan Strait is comparable to that in the Kuroshio onshore intrusion, nutrient transport is only approximately one-tenth of that in the Kuroshio due to low nutrient concentrations.

Compared to those of other sources, the nutrient transport from the Kuroshio Current is substantially greater. The Kuroshio branch southwest of Kyushu is an important component of the Kuroshio onshore intrusion and is also a significant source of the Tsushima Warm Currents, particularly in the fall (Isobe, 1999). The Kuroshio contributes the most to nutrient transport in the TS due to its high nutrient concentrations and proximity to direct intrusion.

4.3 *Which nutrient source contributes significantly to the JS ecosystem?*

The results of our model can provide an explanation for the origins of the nutrients in the TS. The impact of nutrients through the TS on the JS has been the subject of some related research. We therefore tried to clarify the effects of nutrient sources from the ECS on the ecosystem of the JS. Judging from the quantity of nutrient transport, it is clear that the nutrients from the Kuroshio through the TS have the greatest impact, particularly the DIP. However, the roles of the nutrients through the TS in the JS may have been somewhat influenced by the timing and location of the transports.

Using a similar tracking technique within a physical-biological coupled model, Onitsuka et al. (2007) studied the effect of nutrients through the TS on the JS. They found that the DIN flux through the WTS supports high primary productivity in the southwestern JS. The nitrogen flux through the ETS determines the surface nutrient conditions in the nearshore area of the Japanese coast. By examining the biogeochemical responses to various DIN fluxes through the TS, Shibano et al. (2019) demonstrated that the DIN through the TS regulates almost 70% of the DIN in the nearshore zone of the JS. The summertime DIN flux

change had the greatest influence on the ecosystem of the JS. Since stratification prevents DIN from being absorbed locally at the TS, DIN through the TS can instead be delivered to a larger region of the JS.

The sources of summer DIN transport are abundant (Fig. 7a), with both DIN_R and DIN_A reaching their maximum. However, these two compounds are primarily concentrated in the upper layer (Fig. 5), suggesting that they may be utilized quickly after entering and have limited impact on the JS. The summer transport of DIN_K is approximately 15 kmol/s (Fig. 7a). Most of the DIN_K is transported between the 50-m and 100-m depth layers (Fig. 5). The elevated chlorophyll concentration in the center of the JS is mostly caused by nutrient transport in this subsurface layer (Shibano et al., 2019). In addition to being completely dominant in terms of transport quantity, the nutrients from the Kuroshio also distribute fairly in the vertical direction to play further roles in the JS.

5 Conclusions

Using a physical-biological model with a tracking technique, we studied the effects of DIN and DIP from ECS sources on nutrients in the TS. The model can reproduce the variations in velocity, temperature, salinity, chlorophyll *a* concentration, DIN concentration, and DIP concentration in the TS. The volume transport through the TS is also comparable to the observations.

Primary production is generally limited by DIN, except in the upper layer, during summer and fall. Among all the DIN sources, the Kuroshio water has the highest concentration, accounting for 90% of the total DIN in most of the section. The maximum Kuroshio-origin nutrient concentration is located at the bottom, while those of nutrients from the atmosphere and rivers are on the surface during summer and autumn. The concentration of DIN from the Taiwan Strait reaches its highest value in the middle layer in autumn. For DIP sources, the dominance of the Kuroshio is more pronounced.

The nutrient flux is primarily northeastward, and the countercurrent is not strong in the TS. The cores of the nutrient fluxes from the rivers and atmospheric deposition occur in the upper layer. The nutrient fluxes in the Kuroshio current are the greatest between depths of 50 m and 100 m under the combined effect of nutrient concentration and velocity. The nutrient transport through the TS exhibits similar seasonal variations, as does the volume transport. The transports of DIN and DIP from the Kuroshio water account for 85% and 90%, respectively, of the total. The transport of nutrients from the Taiwan Strait is greater during autumn and winter. The transport of DIN from both the atmosphere and rivers peaks in August.

Nutrient transport cannot be equated with volume transport. The DINs in the less saline zone originate not only from rivers but also from atmospheric deposition and the Kuroshio. The transport of nutrients from the Taiwan Strait is not as significant as its volume transport in the TS. The nutrients from the Kuroshio Current, which have the greatest nutrient transport capacity and are mainly distributed in the subsurface layer, have a profound impact on the JS.

References

Bi Rong, Chen Xi, Zhang Jing, et al. 2018. Water mass control on phytoplankton spatiotemporal variations in the northeastern East China Sea and the western Tsushima Strait revealed by lipid biomarkers. Journal of Geophysical Research: Biogeosciences, 123(4): 1318–1332, doi: 10.1002/2017JG004340

Chang PH, Isobe A. 2003. A numerical study on the Changjiang diluted water in the Yellow and East China Seas. Journal of Geophysical Research: Oceans, 108(C9): 3299

Chen Changsheng, Beardsley R C, Limeburner R, et al. 1994. Comparison of winter and summer hydrographic observations in the Yellow and East China Seas and adjacent Kuroshio during 1986. Continental Shelf Research, 14(7-8): 909–929, doi: 10.1016/0278-4343(94)90079-5

Cho Y K, Seo G H, Choi B J, et al. 2009. Connectivity among straits of the northwest Pacific marginal seas. Journal of Geophysical Research: Oceans, 114(C6): C06018

Chung C S, Hong G H, Kim S H, et al. 1998. Shore based observation on wet deposition of inorganic nutrients in the Korean Yellow Sea coast. The Yellow Sea, 4: 30–39

Große F, Fennel K, Zhang Haiyan, et al. 2020. Quantifying the contributions of riverine vs. oceanic nitrogen to hypoxia in the East China Sea. Biogeosciences, 17(10): 2701–2714, doi: 10.5194/bg-17-2701-2020

Guo Xinyu, Miyazawa Y, Yamagata T. 2006. The Kuroshio onshore intrusion along the shelf break of the East China Sea: the origin of the Tsushima Warm Current. Journal of Physical Oceanography, 36(12): 2205–2231, doi: 10.1175/JPO2976.1

Guo Xinyu, Zhu Xiaohua, Wu Qingsong, et al. 2012. The Kuroshio nutrient stream and its temporal variation in the East China Sea. Journal Geophysical Research: Ocean, 117(C1): C01026

Ichikawa H, Beardsley R C. 2002. The current system in the Yellow and East China Seas. Journal of Oceanography, 58(1): 77–92, doi: 10.1023/A:1015876701363

Isobe A. 1999. On the origin of the Tsushima Warm Current and its seasonality. Continental Shelf Research, 19(1): 117–133, doi: 10.1016/S0278-4343(98)00065-X

Isobe A, Ando M, Watanabe T, et al. 2002. Freshwater and temperature transports through the Tsushima-Korea Straits. Journal of Geophysical Research: Oceans, 107(C7): 2-1–2-20

Jin Haoyu, Zhang Chao, Meng Siyu, et al. 2024. Atmospheric deposition and river runoff stimulate the utilization of dissolved organic phosphorus in coastal seas. Nature Communications, 15(1): 658, doi: 10.1038/s41467-024-44838-7

Kim S K, Chang K I, Kim B, et al. 2013. Contribution of ocean current to the increase in N abundance in the Northwestern Pacific marginal seas. Geophysical Research Letters, 40(1): 143–148, doi: 10.1029/2012GL054545

Kim T W, Lee K, Najjar R G, et al. 2011. Increasing N abundance in the northwestern Pacific Ocean due to atmospheric nitrogen deposition. Science, 334(6055): 505–509, doi: 10.1126/science.1206583

Kim H C, Yamaguchi H, Yoo S, et al. 2009. Distribution of Changjiang Diluted Water detected by satellite chlorophyll-*a* and its interannual variation during 1998–2007. Journal of Oceanography, 65(1): 129–135, doi: 10.1007/s10872-009-0013-0

Kodama T, Morimoto A, Takikawa T, et al. 2017. Presence of high nitrate to phosphate ratio subsurface water in the Tsushima Strait during summer. Journal of Oceanography, 73(6): 759–769, doi: 10.1007/s10872-017-0430-4

Kodama T, Setou T, Masujima M, et al. 2015. Intrusions of excess nitrate in the Kuroshio subsurface layer. Continental Shelf Research, 110: 191–200, doi: 10.1016/j.csr.2015.10.012

Kwak J H, Lee S H, Hwang J, et al. 2014. Summer primary productivity and phytoplankton community composition driven by different hydrographic structures in the East/Japan Sea and the Western Subarctic Pacific. Journal of Geophysical Research: Oceans, 119(7): 4505–4519, doi: 10.1002/2014JC009874

Lee J Y, Kang D J, Kim I N, et al. 2009. Spatial and temporal variability in the pelagic ecosystem of the East Sea (Sea of Japan): A review. Journal of Marine Systems, 78(2): 288–300, doi: 10.1016/j.jmarsys.2009.02.013

Lie H J, Cho C H. 2016. Seasonal circulation patterns of the Yellow and East China Seas derived from satellite-tracked drifter trajectories and hydrographic observations. Progress in Oceanography, 146: 121–141, doi: 10.1016/j.pocean.2016.06.004

Liu Sumei, Hong G H, Zhang Jing, et al. 2009. Nutrient budgets for large Chinese estuaries. Biogeosciences, 6(10): 2245–2263, doi:

10.5194/bg-6-2245-2009

Liu Sumei, Zhang Jing, Chen Hongtao. 2000. Chemical oceanography of bioactive elements in the Yellow Sea and the East China Sea. Marine Environmental Science (in Chinese), 19(1): 68–74

Ménesguen A, Cugier P, Leblond I. 2006. A new numerical technique for tracking chemical species in a multi-source, coastal ecosystem, applied to nitrogen causing ulva blooms in the Bay of Brest (France). Limnology and Oceanography, 51(1part2): 591–601, doi: 10.4319/lo.2006.51.1_part_2.0591

Morimoto A, Takikawa T, Onitsuka G, et al. 2009. Seasonal variation of horizontal material transport through the eastern channel of the Tsushima Straits. Journal of Oceanography, 65(1): 61–71, doi: 10.1007/s10872-009-0006-z

Onitsuka G, Yanagi T, Yoon J H. 2007. A numerical study on nutrient sources in the surface layer of the Japan Sea using a coupled physical-ecosystem model. Journal of Geophysical Research: Oceans, 112(C5): C05042

Shen Jiawei, Zhao Liang, Zhang Honghai, et al. 2021. Controlling factors of annual cycle of dimethylsulfide in the Yellow and East China seas. Marine Pollution Bulletin, 169: 112517, doi: 10.1016/j.marpolbul.2021.112517

Shibano R, Morimoto A, Takayama K, et al. 2019. Response of lower trophic ecosystem in the Japan Sea to horizontal nutrient flux change through the Tsushima Strait. Estuarine, Coastal and Shelf Science, 229: 106386

Shin H R, Lee J H, Kim C H, et al. 2022. Long-term variation in volume transport of the Tsushima warm current estimated from ADCP current measurement and sea level differences in the Korea/Tsushima Strait. Journal of Marine Systems, 232: 103750, doi: 10.1016/j.jmarsys.2022.103750

Skogen M D, Søiland H. 1998. A user's guide to NORVECOM v2.0: The Norwegian ecological model system. Institute of Marine Research, 42, https://core.ac.uk/outputs/30846984/[1998-01-01/2022-05-23]

Skogen M D, Svendsen E, Berntsen J, et al. 1995. Modelling the primary production in the North Sea using a coupled three-dimensional physical-chemical-biological ocean model. Estuarine, Coastal and Shelf Science, 41(5): 545–565

Takikawa T, Yoon J H, Cho K D. 2005. The Tsushima warm current through Tsushima Straits estimated from ferryboat ADCP data. Journal of Physical Oceanography, 35(6): 1154–1168, doi: 10.1175/JPO2742.1

Teague W J, Jacobs G A, Ko D S, et al. 2003. Connectivity of the Taiwan, Cheju, and Korea straits. Continental Shelf Research, 23(1): 63–77, doi: 10.1016/S0278-4343(02)00150-4

Umezawa Y, Yamaguchi A, Ishizaka J, et al. 2014. Seasonal shifts in the contributions of the Changjiang River and the Kuroshio current to nitrate dynamics in the continental shelf of the northern East China Sea based on a nitrate dual isotopic composition approach. Biogeosciences, 11(4): 1297–1317, doi: 10.5194/bg-11-1297-2014

Wang Yucheng, Guo Xinyu, Zhao Liang, et al. 2019. Seasonal variations in nutrients and biogenic particles in the upper and lower layers of East China Sea Shelf and their export to adjacent seas. Progress in Oceanography, 176: 102138, doi: 10.1016/j.pocean.2019.102138

Wu Wentao, Wang Junjie, Wang Hao, et al. 2023. Trends in nutrients in the Changjiang River. Science of the Total Environment, 872: 162268, doi: 10.1016/j.scitotenv.2023.162268

Yamada K, Ishizaka J, Nagata H. 2005. Spatial and temporal variability of satellite primary production in the Japan Sea from 1998 to 2002. Journal of Oceanography, 61(5): 857–869, doi: 10.1007/s10872-006-0005-2

Yanagi T. 2002. Water, salt, phosphorus and nitrogen budgets of the Japan Sea. Journal of Oceanography, 58(6): 797–804, doi: 10.1023/A:1022815027968

Zhang Jing. 1996. Nutrient elements in large Chinese estuaries. Continental Shelf Research, 16(8): 1023–1045, doi: 10.1016/0278-4343(95)00055-0

Zhang Jing, Guo Xinyu, Zhao Liang. 2019. Tracing external sources of nutrients in the East China Sea and evaluating their contributions to primary production. Progress in Oceanography, 176: 102122, doi: 10.1016/j.pocean.2019.102122

Zhang Jing, Guo Xinyu, Zhao Liang. 2021. Budget of riverine nitrogen over the East China Sea shelf. Environmental Pollution, 289: 117915, doi: 10.1016/j.envpol.2021.117915

Zhang Jing, Liu Minguang. 1994. Observations on nutrient elements and sulphate in atmospheric wet depositions over the northwest Pacific coastal oceans—Yellow Sea. Marine Chemistry, 47(2): 173–189, doi: 10.1016/0304-4203(94)90107-4

Zhang Jing, Liu Sumei, Ren Jingling, et al. 2007. Nutrient gradients from the eutrophic Changjiang (Yangtze River) Estuary to the oligotrophic Kuroshio waters and re-evaluation of budgets for the East China Sea Shelf. Progress in Oceanography, 74(4): 449–478, doi: 10.1016/j.pocean.2007.04.019

Zhang Renjian, Wang Mingxing, Sheng Lifang, et al. 2004. Seasonal characterization of dust days, mass concentration and dry deposition of atmospheric aerosols over Qingdao, China. China Particuology, 2(5): 196–199, doi: 10.1016/S1672-2515(07)60058-X

Zhang Jing, Zhang Guosen, Bi Y F, et al. 2011. Nitrogen species in rainwater and aerosols of the Yellow and East China seas: Effects of the East Asian monsoon and anthropogenic emissions and relevance for the NW Pacific Ocean. Global Biogeochemical Cycles, 25(3): GB3020

Zhao Liang, Guo Xinyu. 2011. Influence of cross-shelf water transport on nutrients and phytoplankton in the East China Sea: A model study. Ocean Science, 7(1): 27–43, doi: 10.5194/os-7-27-2011